Appl. Phys. B 66, 169–173 (1998)

Applied Physics B
Lasers
and Optics
© Springer-Verlag 1998

Determination of dispersion characteristics in anisotropic materials using ultrashort pulses

H. Delbarre, C. Przygodzki, W. Chen, D. Boucher

Laboratoire de Physico-Chimie de l'Atmosphère, Université du Littoral, M.R.E.I.D. 145, route du Pertuis d'Amont, 59140 Dunkerque, France
(Fax: +33-3/2865-8244, E-mail: delb@hplamer.univ-littoral.fr)

Received: 11 February 1997/Revised version: 23 May 1997

Abstract. Stoichiometric conditions have been shown to influence substantially the dispersion characteristics of birefringent crystals. We have investigated a temporal method using ultrashort pulse propagation to determine the dispersion constants in the visible spectrum, and the method was applied to the characterization of an $AgGaS_2$ crystal. This method, based on group velocity measurement, allows the determination of the principal axes, the indices, the group velocities and the group velocity dispersion (GVD).

PACS: 42.70; 42.80

For parametric processes involving ultrashort light pulses, it is important to have not only a precise knowledge of both extraordinary and ordinary indices (for uniaxial crystals) of the medium, because of the phase-matching condition requirements, but it is also necessary to estimate precisely the group velocities $V_g(\omega) = (\mathrm{d}k/\mathrm{d}\omega)^{-1}$. These determine the interaction length of the pulses and the group velocity dispersion (GVD) $k''(\omega) = \left(\mathrm{d}^2k/\mathrm{d}\omega^2\right) = -(1/V_g^2) \times \left(\mathrm{d}V_g/\mathrm{d}\omega\right)$ which gives rise to the self-temporal broadening of pulses during propagation.

The determination of these characteristics can be achieved in two different ways: First, a precise knowledge of the refractive index is sufficient as a rule to obtain an estimation of the group velocity and the GVD. The experimental data fitted by Sellmeier equations for silver thiogallate ($AgGaS_2$) given in most references provide different values (discrepancy of the order of 0.3%), although each of them offer a good relative precision on the fit (about 0.01%). We are not able to define clearly the origin of these differences but it appears that the stoichiometric composition might be different from one crystal to another [1]. In this context, it is difficult to speak about relevant data for the group velocity and the GVD (respectively the first and second order derivatives of the index with respect to wavelength) without direct measurements of the actual crystal sample.

Usually, index measurements are performed with continuous wave (cw) light sources. The index can be determined by a spatial method using prism light deviation [1, 2]; but this method implies a particular cutting of the sample. So, the "measured crystal" cannot be the crystal used in actual experiments.

Interference in the spectral domain with a white light source has also been used recently [3, 4]. It is a very precise method (absolute accuracy of the order of 10^{-5}) for index retrieval of isotropic crystals. However, it is not obvious here how to apply this method to birefringent crystals, because it does not allow a direct determination of the principal axes and it requires a crystal surface quality of better than $\lambda/2$ [3]. Moreover, one could think of applying this method with standard femtosecond sources by using the techniques usually devoted to pulse features characterization [5]. However, the "narrow" bandwidth (4–20 nm) of standard femtosecond sources (50–100 fs) would only provide local spectral information on the dispersion characteristics and it would be difficult to retrieve reliable index coefficients from such a narrow interferogram.

Finally, the index can be retrieved [6, 7], or at least improved [8–12] from an analysis of phase-matching conditions in a particular parametric process. Realistic and relevant data can also be obtained by a correct weighting of data provided by different types of measurements [13].

We suggest a second complementary approach which consists of using ultrashort pulses for a direct group velocity measurement by a temporal method following the pioneering work of Hirlimann et al. [14] on group delay measurements. This method requires the use of an autocorrelator (modified Michelson interferometer) and a monochromator (spectrometer).

This will permit the following :
(i) easy determination of the orientation of the ordinary and extraordinary axes;
(ii) direct measurement of group velocities;
(iii) easily retrieval of the refractive indices;
(iv) derivation of the GVD from the group velocities.

1 The temporal method

1.1 Experimental device

The idea for measuring group velocity consists of comparing the propagation time of ultrashort pulses (about 100 fs)

through the crystal with the propagation time along the same length in air. For this purpose, we use a standard autocorrelator using a KDP doubling crystal in a "background free" intensimetric configuration (Fig. 1). The carrier wavelength is measured with a monochromator that has a 0.1 nm wavelength precision. The pulses are produced by a β-barium-borate (BBO) Type I optical parametric amplifier (OPA), operating in the 0.5–0.7 micron range and pumped with microjoule 400-nm-wavelength pulses from a 200-kHz Ti:sapphire regenerative amplifier system. A diffraction-limited white-light continuum produced in sapphire is used as a low-energy signal seed. The amplified signal pulses have a Gaussian shape with a typical energy of 100 nJ, a mean temporal width (FWHM) of 100 fs and a bandwidth that ranges from 5 to 10 nm. The beam intensity has been attenuated by one order of magnitude to avoid any eventual two-photon absorption of the crystal in the visible range (this is the reason why the intercorrelation trace in Fig. 2 is noisy).

First of all, the zero delay between both arms is adjusted without the sample by optimizing the autocorrelation signal. Figure 2 shows a typical intensimetric autocorrelation function obtained with 100 fs transform-limited Gaussian pulses. The sample is a 1.29 mm thick $AgGaS_2$ crystal cut at $\theta_c = 90°$ for use in non-critical phase-matching (NCPM) frequency

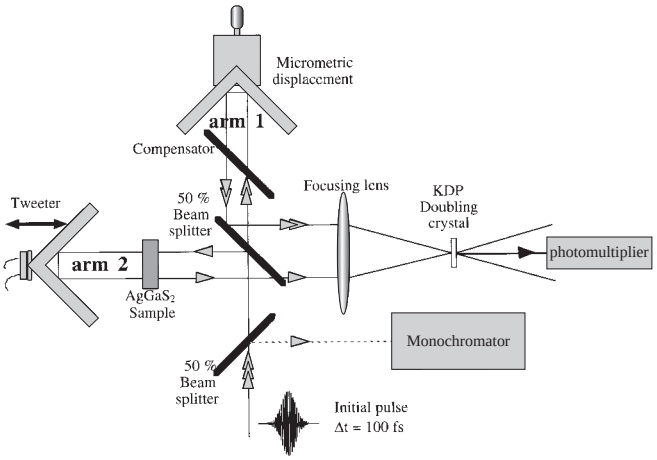

Fig. 1. Schematic experimental layout for compensation length measurement

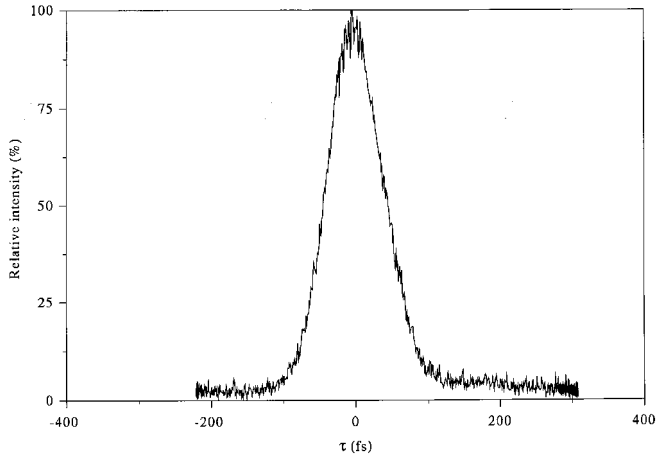

Fig. 2. Typical experimental intensimetric autocorrelation trace

mixing experiments [15, 16]. The focusing of a small-range microscope allows an accurate measurement of the crystal thickness with a 5 micron precision. Besides, the actual value has been confirmed numerically by seeding the thickness as a varying parameter in the nonlinear fit procedure. The principal axes of the crystal are normal to the wave vector of the incident field. The crystal is placed perpendicular to the injected beam in arm 2, and its position is optimized by tilting it, in order to superpose the incident and back-reflected light from the input face. The pulse coming from arm 2 is delayed with respect to its twin pulse coming from the other arm. The first arm length can be adjusted with an accuracy of $\pm$ 5 μm ($\sim$ 17 fs) in order to find the zero delay. The ordinary (extraordinary) axis can be selected by minimizing (maximizing) this compensation length on the free arm 1 at a given wavelength ($\lambda = 540$ nm) with correct positioning of the crystal towards the incident wave.

The experimental parameters and uncertainties for the crystal and compensation lengths are given in Table 1.

Let us now examine the way to find the group velocity, the index and GVD using the compensation length experimental measurements.

1.2 Dispersion characteristics

An adjustment of the dispersion parameters is realized using the standard Levenberg–Marquardt nonlinear fit procedure [17]. As a reference, we considered the experimental results for the $AgGaS_2$ crystal in [1, 6, 7, 18]. The indices are given by the following Sellmeier equations for the ordinary (o) and extraordinary (e) indices:

$$n_{o,e}^{ref} = \sqrt{A_{o,e}^{ref} + \frac{B_{o,e}^{ref}}{1 - C_{o,e}^{ref}/\lambda^2} - D_{o,e}^{ref}\lambda^2}\,. \tag{1}$$

The reference values of the parameters are given in Table 2. A specific procedure has been developed for each of the dispersion characteristics.

1.2.1 Direct group velocity measurements. It is easy to show, by examining the time delays, that the "compensated length" ℓ_{comp} on the free arm is related to the group velocity V_g in the crystal as follows:

$$\ell_{comp}(\lambda) = L_{eff.}\left(\frac{V_{air}}{V_g(\lambda)} - 1\right)\,. \tag{2}$$

Table 1. Experimental parameters

Quantity	Designation	Experimental value
$AgGaS_2$ crystal length	$L_{crystal}$	1.290 mm
Uncertainty on the length	$\Delta L_{crystal}$	±5 μm
Uncertainty on compensated length	$\Delta\ell_{comp}$	±5 μm
Uncertainty on the wavelength	$\Delta\lambda$	±0.1 nm
Scanned spectral range	$[\lambda_{min}; \lambda_{max}]$	[0.5; 0.7] μm
Cut angle of the crystal	θ_c	$(\pi/2)$ rad

Table 2. Reference parameters for $AgGaS_2$ indices

Parameter	Reference I [18]	Reference II [6]	Reference III [1]	Reference IV [7]
A_o^{ref}	2.958	3.3970	4.6187	3.6280
B_o^{ref}	2.770	2.3982	1.3758	2.1686
C_o^{ref} (μm^2)	0.08703	0.09311	0.1205	0.1003
D_o^{ref} (μm^{-2})	0.00210	0.00228	0.2098	0.00229
A_e^{ref}	3.947	3.5873	5.5373	4.0172
B_e^{ref}	1.550	1.9533	0.5685	1.5274
C_e^{ref} (μm^2)	0.1307	0.11066	0.1725	0.1310
D_e^{ref} (μm^{-2})	0.00233	0.00227	0.6704	0.00228

Hence the experimental measurements of ℓ_{comp} lead to direct knowledge of the group velocity:

$$V_g(\lambda) = \frac{V_{air} \cdot L_{eff}}{(\ell_{comp}(\lambda) + L_{eff})} . \quad (3)$$

where $L_{eff} = 2 \times L_{crystal}$ is the effective length of the crystal used in the measurements and $V_{air} \simeq C/n_{air}$ is the group velocity of the pulses in air.

The experimental compensation lengths for the ordinary and extraordinary axes are depicted in Fig. 3. The compensation length is a simple function of the wavelength, and in order to eliminate the points dispersion, it is useful to fit the compensation length with a third-order polynomial:

$$\ell_{comp} = a_0 + a_1\lambda + a_2\lambda^2 + a_3\lambda^3 . \quad (4)$$

The fitted coefficient values and their corresponding uncertainties are given in Table 3 and the corresponding fit curves are displayed in Fig. 3.

The ordinary and extraordinary curves cross at $\lambda \simeq 620$ nm. Therefore, it is necessary to select a wavelength far away from the crossing point of the curves to discriminate the ordinary and extraordinary axes by optimizing the compensating length. This is the reason why we have chosen the lower wavelength $\lambda = 540$ nm for positioning the ordinary or extraordinary axes.

Table 3. Fitted parameters for group velocity retrieval

Parameter	Fitted value
$a_0^o \pm \Delta a_0^o$	$30.0237 \pm 6.0 \times 10^{-4}$ mm
$a_1^o \pm \Delta a_1^o$	$-88.486 \pm 1.0 \times 10^{-3}$ mm/μm
$a_2^o \pm \Delta a_2^o$	$119.308 \pm 1.5 \times 10^{-3}$ mm/μm^2
$a_3^o \pm \Delta a_3^o$	$-54.804 \pm 2.5 \times 10^{-3}$ mm/μm^3
$a_0^e \pm \Delta a_0^e$	$47.972 \pm 5.0 \times 10^{-4}$ mm
$a_1^e \pm \Delta a_1^e$	$-167.916 \pm 9.0 \times 10^{-4}$ mm/μm
$a_2^e \pm \Delta a_2^e$	$237.012 \pm 1.5 \times 10^{-3}$ mm/μm^2
$a_3^e \pm \Delta a_3^e$	$-113.308 \pm 2.3 \times 10^{-3}$ mm/μm^3

The ordinary group velocity V_g^o deduced from the compensation length is displayed in Fig. 4. This figure contains also the group velocities obtained from the reference data.

The uncertainty on the group velocity is calculated according to the uncertainty in the fitting coefficients:

$$\Delta V_g \simeq \sum_{i=0}^{3} \left(\left| \frac{\partial V_g}{\partial a_i} \right| \Delta a_i \right) + \left| \frac{\partial V_g}{\partial \lambda} \right| \Delta\lambda + \left| \frac{\partial V_g}{\partial L_{eff}} \right| \Delta L_{eff} . \quad (5)$$

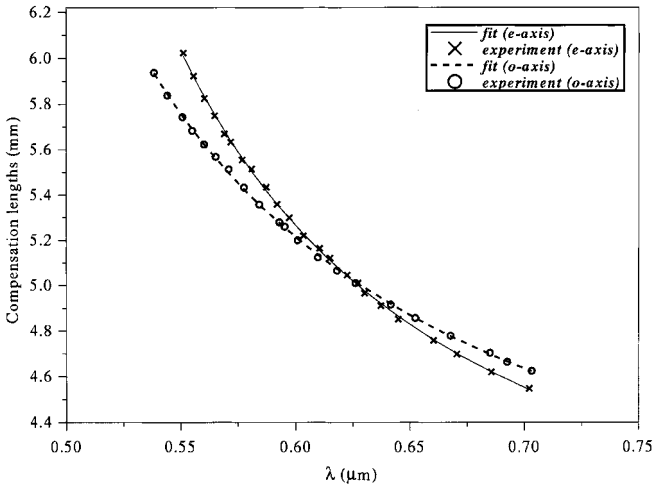

Fig. 3. Experimental measurements of the compensation length for ordinary and extraordinary axes. The fitted values are also displayed

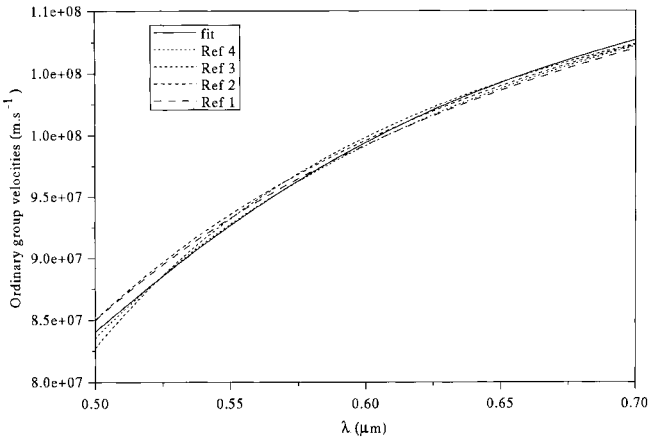

Fig. 4. Comparison between the fitted values for the ordinary group velocity and the reference data derived from Table 2

The uncertainties of the fitting coefficients Δa_i (Table 3) are computed independently in order to ensure a 99% confidence level.

The relative uncertainty on the ordinary group velocity ($\Delta V_g^o/V_g^o$) (displayed in Fig. 7) remains below 0.1%. This can be compared with the relative gap (which is greater than 2% for some wavelengths) between the four data sets obtained by first-order derivative calculations of (1). It appears that it is necessary to measure directly the group velocities of the sample itself rather than deducing them from precise reference indices measured for different crystals: the derivation increases the discrepancy between the various references.

1.2.2 Refractive index calculation. In the normal dispersion regime ($\mathrm{d}n/\mathrm{d}\lambda \leq 0$), the group velocity of an optical pulse is related to the index via a first-order derivative:

$$V_g(\lambda) = \frac{1}{\mathrm{d}k/\mathrm{d}\omega} = \frac{C}{n(\lambda) - \lambda\,(\mathrm{d}n/\mathrm{d}\lambda)}\,. \tag{6}$$

The index is then determined by integrating the first-order differential equation:

$$n(\lambda) - \lambda\left(\frac{\mathrm{d}n}{\mathrm{d}\lambda}\right) = n_{\mathrm{air}}\left(\frac{\ell_{\mathrm{comp}}(\lambda)}{L_{\mathrm{eff}}} + 1\right) \tag{7}$$

where a direct integration provides the solution:

$$n(\lambda) = n_{\mathrm{air}} + (n_0 - n_{\mathrm{air}})\left(\frac{\lambda}{\lambda_0}\right) - n_{\mathrm{air}}\lambda\int_{\lambda_0}^{\lambda}\frac{\ell_{\mathrm{comp}}(x)}{x^2 L_{\mathrm{eff}}}\,\mathrm{d}x\,. \tag{8}$$

Of course, the refractive index is only defined to the nearest constant $n_0 = n(\lambda_0)$. If a precise index n_0 is known at a specific wavelength λ_0, the index at any wavelength is determined by integration of the compensation length. But this is not generally the case. However, a solution can be found without any reference constant, by specifying a particular spectral dependence for the index. In practice, we adopt the classical Sellmeier expression for the index given in (1). This form is then derived in the compensation length formulation:

$$\ell_{\mathrm{comp}}^{\mathrm{o,e}} = \frac{L_{\mathrm{eff}}}{n_{\mathrm{air}}}\left(n_{\mathrm{o,e}} - \lambda\left(\frac{\mathrm{d}n_{\mathrm{o,e}}}{\mathrm{d}\lambda}\right) - n_{\mathrm{air}}\right)\,. \tag{9}$$

Finally, a fit is performed on the experimental compensation length by using the preceding expression. This fit yields the coefficients $A_{\mathrm{o,e}}$, $B_{\mathrm{o,e}}$, $C_{\mathrm{o,e}}$ displayed in Table 4. The infrared parameters $D_{\mathrm{o,e}}$ have been neglected in the fit procedure because they are not relevant in the measurement range (0.5–0.7) μm. The spectral dependence of the ordinary index n_{o} is displayed in Fig. 5 (solid line for the fit and dotted lines for the reference data). Our fitted curve is in agreement with the reference data (with a maximum relative discrepancy equal to 0.3%). We have used the same procedure as previously for computing the relative uncertainty on the index ($\Delta n_{\mathrm{o}}/n_{\mathrm{o}}$). Figure 7 shows that this uncertainty remains below 3.0×10^{-4} for a confidence level of 99% on each parameter A_{o}, B_{o}, C_{o}. We obtain accuracies of the same order for the extraordinary axis.

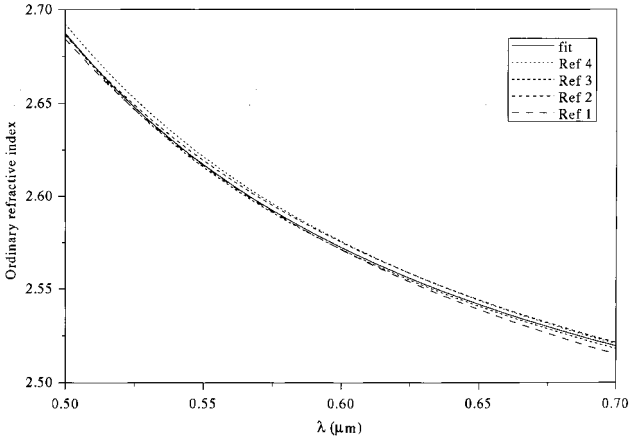

Fig. 5. Comparison between the fitted values for the ordinary refractive index and the reference data given in Table 2

Table 4. Fitted parameters for refractive index retrieval

Parameter	Fitted value
$A_{\mathrm{o}} \pm \Delta A_{\mathrm{o}}$	$3.917 \pm 1.6\times10^{-3}$
$B_{\mathrm{o}} \pm \Delta B_{\mathrm{o}}$	$1.905 \pm 5.7\times10^{-4}$
$C_{\mathrm{o}} \pm \Delta C_{\mathrm{o}}$	$0.10596 \pm 2.7\times10^{-5}$ μm^2
$A_{\mathrm{e}} \pm \Delta A_{\mathrm{e}}$	$4.414 \pm 1.3\times10^{-3}$
$B_{\mathrm{e}} \pm \Delta B_{\mathrm{e}}$	$1.2288 \pm 3.3\times10^{-4}$
$C_{\mathrm{e}} \pm \Delta C_{\mathrm{e}}$	$0.13833 \pm 3.0\times10^{-5}$ μm^2

1.2.3 Determination of the GVD factors. It is usual to define a second-order dispersion factor by the quantity:

$$k'' = \left(\frac{\mathrm{d}^2k}{\mathrm{d}\omega^2}\right) = \frac{-1}{V_g^2}\left(\frac{\mathrm{d}V_g}{\mathrm{d}\omega}\right) \tag{10}$$

which can be directly expressed in terms of the experimental data ℓ_{comp} by the formula:

$$k'' = -n_{\mathrm{air}}\frac{\lambda^2}{2\pi C^2 L_{\mathrm{eff}}}\left(\frac{\mathrm{d}\ell_{\mathrm{comp}}}{\mathrm{d}\lambda}\right)\,. \tag{11}$$

In this case, the GVD factor k'' is represented by a third-order polynomial in the spectral domain.

$$k'' = \alpha + \beta\lambda + \gamma\lambda^2 + \delta\lambda^3\,. \tag{12}$$

This expression can be integrated using (11) in order to fit the experimental ℓ_{comp} measurements with the following expression:

$$\ell_{\mathrm{comp}} = -\frac{2\pi C^2 L_{\mathrm{eff}}}{n_{\mathrm{air}}}\left(-\frac{\alpha}{\lambda} + \beta\ln(\lambda) + \gamma\lambda + \frac{\delta}{2}\lambda^2\right) + \epsilon\,. \tag{13}$$

The numerical values of the fitting parameters are gathered in Table 5. The deduced GVD factors k_{o}'' and the corresponding relative accuracies are shown respectively on Figs. 6 and 7 for the ordinary axis. The maximum

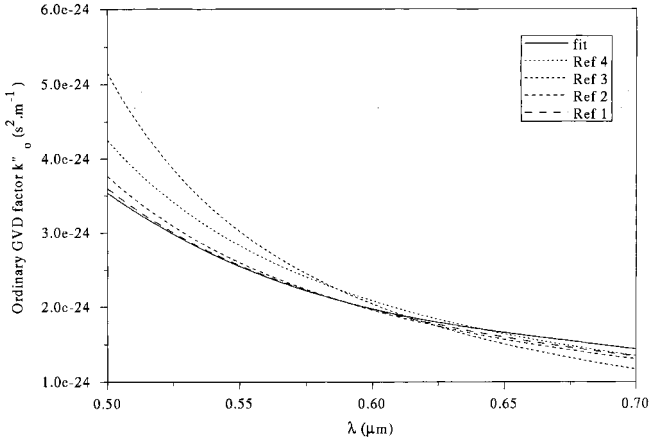

Fig. 6. Comparison between the fitted values for the ordinary GVD factor and the reference data derived from Table 2

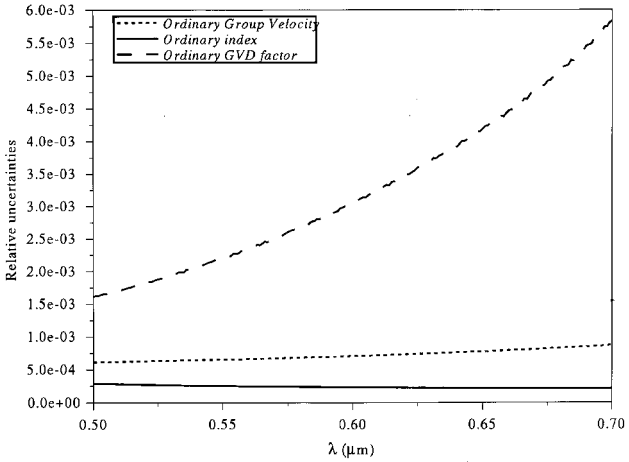

Fig. 7. Calculated relative uncertainties of the fitted group velocity, index, and Group Velocity Dispersion factor for the ordinary axis

Table 5. Fitted parameters for GVD factor retrieval

Parameter	Fitted value
$\alpha_o \pm \Delta\alpha_o$	$7.1931 \times 10^{-23} \pm 1.0 \times 10^{-28}$ s^2/m
$\beta_o \pm \Delta\beta_o$	$-3.02344 \times 10^{-16} \pm 4.2 \times 10^{-22}$ s^2/m^2
$\gamma_o \pm \Delta\gamma_o$	$4.3879 \times 10^{-10} \pm 2.0 \times 10^{-15}$ s^2/m^3
$\delta_o \pm \Delta\delta_o$	$-2.1533 \times 10^{-4} \pm 1.9 \times 10^{-8}$ s^2/m^4
$\alpha_e \pm \Delta\alpha_e$	$3.21740 \times 10^{-22} \pm 3.0 \times 10^{-28}$ s^2/m
$\beta_e \pm \Delta\beta_e$	$-1.44400 \times 10^{-15} \pm 1.0 \times 10^{-22}$ s^2/m^2
$\gamma_e \pm \Delta\gamma_e$	$2.19029 \times 10^{-9} \pm 1.1 \times 10^{-15}$ s^2/m^3
$\delta_e \pm \Delta\delta_e$	$-1.11583 \times 10^{-3} \pm 4.2 \times 10^{-9}$ s^2/m^4

relative accuracy ($\Delta k''_o/k''_o$) is of the order of 0.6%; it is larger than the relative accuracy obtained for the indices and group velocities. Moreover, the results obtained with the reference data strongly diverge (about 40% at $\lambda \simeq 500$ nm).

2 Discussion and conclusion

The temporal method provides a good scheme for the determination of indices, group velocities and GVD constants of any crystal. In addition, it allows a direct determination of the principal axes of a birefringent medium by maximizing or minimizing the compensation length. As an application, we have studied the dispersion features of an $AgGaS_2$ crystal and obtained relative accuracies respectively of the order of 3.0×10^{-4} for the indices, below 1.0×10^{-3} for the group velocities, and about 6.0×10^{-3} for the GVD factors. This method is more suited for group velocity and GVD measurements than the second-order derivation of indices which generally amplify the errors.

Some technical improvements are achievable for increasing the accuracy. First of all, the accuracy for the determination of the zero delay position in the Michelson interferometer can be considerably enhanced by using an interferometric method, rather than an intensimetric one. In this way, a first-order autocorrelation would be well suited if the compensation length measurement and the signal-to-noise ratio are also improved.

Secondly, a knowledge of the crystal thickness can be improved by using the internal reflections in the crystal and measuring the corresponding compensation lengths. Finally, this method can be applied for longer crystals, but cannot be applied for very thin media: the lower limit is determined by the pulse length which is about 30 μm for a 100 fs duration.

Acknowledgements. We are very grateful to Professor F.K. Tittel for encouragement and very useful comments concerning the manuscript.

The Laboratoire de Physicochimie de l'Atmosphère participates in the Centre d'Etudes et de Recherches Lasers et Applications, supported by the Ministère chargé de la Recherche, the Région Nord/Pas de Calais, and the Fonds Européen de Développement Economique des Régions. This work has also benefited from the financial support of the Centre de Développement et de Recherche pour le Commerce et l'Industrie of Dunkerque.

References

1. G.C. Bahr, R.C. Smith: IEEE J. Quantum Electron. QE-**10**, 546 (1974)
2. G.D. Boyd, H. Kasper, J.H. McFee: IEEE J. Quantum Electron. QE-**7**, 563 (1971)
3. C. Sainz, P. Jourdain, R. Escalona, J. Calatroni: Opt. Commun. **110**, 381 (1994)
4. V. Nirmal Kumar, D. Narayana Rao: J. Opt. Soc. Am. B **12**, 1559 (1995)
5. L. Lepetit, G. Chériaux, M. Joffre: J. Opt. Soc. Am. B **12**, 2467 (1995)
6. Yuan Xuan Fan, R.C. Eckardt, R.L. Byer, R.K. Route, R.S. Feigelson: Appl. Phys. Lett. **45**, 313 (1984)
7. G.C. Bhar: Appl. Opt. **15**, 305 (1976)
8. P. Canarelli, Z. Benko, A.H. Hielscher, R.F. Curl, F.K. Tittel: IEEE J. Quantum Electron. QE-**28**, 52 (1992)
9. K. Kato: IEEE J. Quantum Electron. QE-**20**, 698 (1984)
10. T. Elsaesser, A. Seilmeier, W. Kaiser, P. Koidl, G. Brandt: Appl. Phys. Lett. **44**, 383 (1984)
11. Toshikazu Itabe, J.L. Bufton: Appl. Opt. **23**, 3044 (1984)
12. R.J. Seymour, F. Zernike: Appl. Phys. Lett. **29**, 705 (1976)
13. D.A. Roberts: Appl. Opt. **35**, 4677 (1996)
14. C. Hirlimann, J.-F. Morhange, M. May: J. Opt. Soc. Am. B **6**, 1899 (1989)
15. U. Simon, F.K. Tittel, L. Goldberg: Opt. Lett. **18**, 1931 (1993)
16. U. Simon, C.E. Miller, C.C. Bradley, R.G. Hulet, R.F. Curl. F.K. Tittel: Opt. Lett. **18**, 1062 (1993)
17. W.H. Press, B.P. Flannery, S.A. Teukolsky, W.T. Vetterling: *Numerical Recipes in Pascal: The Art of Scientific Computing*, 3rd edn. (Cambridge University Press, New York 1992), pp. 572–598
18. E.C. Cheung, J.M. Liu: J. Opt. Soc. Am. B **8**, 1491 (1991)